Scattering and absorption in 2D optics

Mariani, F.

Chapter 4

Scattering media characterization with phase-only wavefront modulation

A new approach for probing the scattering properties of complex media is proven experimentally. Using phase-only modulation of the light illuminating a random scattering sample, we induce and record fluctuations in the reflected speckle patterns. Using predictions from diffusion theory, we obtain the scattering and absorption coefficients of the sample from the average change in the speckle amplitude. Our approach, which is based on interference, is in principle able to give better signal to noise ratio as compared to an intensity modulation approach. We compare our results with those obtained from a knife-edge illumination method and enhanced back-scattering cone. Our work can find application in the non-invasive study of biological specimens as well as the study of light propagation in random scattering devices like solar cells or LEDs.

This chapter is submitter for publication as:
F. Mariani, W. Loeffler, M. Aas, O. S. Ojambati, P. Hong, W. L. Vos and M. P. van Exter, Optics Express (2017)

4.1 Complex scattering media

Complex scattering media are ubiquitous, spanning from artifical ones like white paint or paper to biological forms like cellular tissue or bones. In all these materials the light propagation is scrambled by multiple scattering events [1], with the effect of a reduced overall transmission when the sample thickness is larger than the transport mean free path, i.e. the average distance before a change in propagation direction occurs. The complexity of the processes happening in scattering media makes these materials challenging and fascinating to study.

Different techniques have been used to characterize optical properties of complex media. Some methods approximate light propagation as a diffusion process, thus neglecting the wave nature of light and the associated interference phenomena; examples of diffusion-based techniques are total transmission measurement [2, 3, 4] and diffuse imaging analysis [5, 6]. Other methods are based on interference and require the light to be treated as a wave. This is the case for the enhanced back-scattering (EBS) technique [7, 8, 9], the analysis of speckles statistics [10] to measure diffusion parameters [11, 12, 13], and the measurements of the transmission matrix [14, 15].

Being able to study the properties of complex media is interesting for fundamental reasons as well as for those applications that require controlling light propagation within the scattering material. Recently, wavefront-shaping techniques have been employed to control the propagation of light in complex media [16, 17] or even produce images of objects positioned beyond opaque screens [18]. Studying how light transport is affected by structural and compositional properties of a medium if of great interest in materials diagnostic and analysis of biological specimens [19], where non-invasive methods are particularly relevant.

In this work we demonstrate a new non-invasive method to measure transport and absorption parameters in three dimensional random scattering media. We spatially modulate the phase of the light illuminating a sample and analyze the intensity variations in the reflected speckle patterns. We interpret the results using an analytic solution of the diffusion equation applied to a semi-infinite complex scattering medium. Compared to diffuse imaging with point-like illumination [6], where transport is studied by measuring diffusion profile, our technique is promising in studying fields that propagate deeper into the sample, is not affected by the direct backscattered light, and does not

require a very large detection dynamic range.

4.2 From diffusion theory to speckles fluctuations

The interaction of coherent light with a random scattering medium produces speckle patterns; these appear to have a random structure [20] which is nonetheless deterministically defined by the structure of the medium. In a linear optical process, such as elastic scattering, the relation between the input field $\mathbf{E}_{\text{in}}(x', y')$ and the reflected field $\mathbf{E}_R(x, y)$ is described by the Green's tensor $\mathbf{G}(x, y, x', y')$:

$$\begin{aligned} \mathbf{E}_R(x,y) &= \mathbf{G}(x,y,x',y') \otimes \mathbf{E}_{\text{in}}(x',y') \equiv \\ &\equiv \iint \mathbf{G}(x,y,x',y')\ \mathbf{E}_{\text{in}}(x',y')\ dx'dy' \end{aligned} \tag{4.1}$$

The method that we introduce in this work is based on optical phase modulation and uses the properties of Eq. (4.1), without requiring any direct knowledge of the Green's function $\mathbf{G}(x, y, x', y')$. We consider the field incident on the sample $\mathbf{E}_{\text{in}}(x', y')$ and divide it into two halves around $x = 0$. By making use of the linearity of Eq. (4.1), we rewrite the reflected field as the sum of two components $\mathbf{E}_R(x, y) = \mathbf{E}_-(x, y) + \mathbf{E}_+(x, y)$, each given by:

$$\mathbf{E}_\pm(x,y) = \mathbf{G}(x,y,x',y') \otimes \left[H(\pm x')\ \mathbf{E}_{\text{in}}(x',y')\right] \tag{4.2}$$

where $H(\pm x')$ is the Heaviside step-function. The functions $\mathbf{E}_{+/-}(x, y)$ represent the field reflected, after propagation, upon illumination with light on only half of the illumination beam for $x > 0$ ("+" case) or $x < 0$ ("-" case); this is sketched in the inset in Fig. 4.1. In the following we consider only one polarization component of $\mathbf{E}_{+/-}$ and write the fields as $E_{+/-}$.

If we introduce an arbitrary phase retardation $\Delta\phi$ in the input beam for e.g. only the half $x < 0$, the field propagation is not affected, but the only results is a phase shift for the output field $E_-(x, y)$ as compared to $E_+(x, y)$. The total reflected field becomes $E_R = e^{i\Delta\phi}E_- + E_+$, with the phase shift $\Delta\phi$ modifying the interference between the two components. The reflected intensity $I_R(x, y) \propto |E_R(x, y)|^2$ at the scattering medium surface is obtained by substituting the expression for $E_R(x, y)$, including the phase retardation $\Delta\phi$:

$$I_R(x,y;\Delta\phi) \propto I_C(x,y) + I_A(x,y)\cos(\Delta\phi + \psi) \tag{4.3}$$

where $I_C = |E_-|^2 + |E_+|^2$, $I_A = 2|E_-^* E_+|$ and $\psi = \arg(E_+/E_-)$, with $E_{+/-}$ complex field amplitudes. The central idea of this work is resumed by Eq. (4.3):

the reflected intensity is locally modified by interference when $\Delta\phi$ is varied in a $[0, 2\pi]$ interval. By recording the intensity variations we can determine both the product of the reflected fields amplitudes and their relative phase. Since scattering and absorption properties of the medium influence the amplitudes of the reflected fields $E_{\pm}(x, y)$, they also determine the profile of $I_A(x, y)$.

To attain a practical use the interference principle in Eq. (4.3) we need to relate the field amplitudes to the scattering and absorption properties of our medium. This is possible looking at averaged results for the reflected intensity, a quantity we can directly measure. The ensemble-averaged reflected intensity $\langle I_{R\pm}(x, y)\rangle$ corresponds to the mean square value for the reflected fields amplitude, hence we can write $\langle |E_{\pm}(x, y)|\rangle \propto \sqrt{\langle I_{R\pm}(x, y)\rangle}$.

While the measured speckle-like reflected intensity $I_R(x, y)$ strongly depends on the precise positions of the scatterers, $\langle I_R(x, y)\rangle$ can be calculated by using a diffusion approximation to describe the transport of optical energy in the medium. This approximation is valid when the transport mean free path l_{tr} for the light in the medium is much smaller than the absorption mean free path l_a and light is backscattered after multiple scattering events [1, 21]. These conditions are fulfilled in our experiment.

The diffusion equation has an analytical solution for a point like source in an infinite scattering medium. This can be used to solve the case for a point-like illumination incident at $x = y = 0$ on the interface of a semi-infinite medium, which yields the radial profile of the diffuse reflected intensity $R(\rho)$ at the interface, with $\rho = \sqrt{x^2 + y^2}$. We use here the expression for $R(\rho)$ from Ref. [5] for a random medium of effective refractive index n_{eff} surrounded by air ($n_{\text{out}} = 1$).

We model the diffuse light as coming from two isotropic point sources [5, 6]: the first is located inside the medium at a depth $z_0 = (\mu_a + \mu'_s)^{-1}$, with $\mu'_s = l_{tr}^{-1}$ and $\mu_a = l_a^{-1}$. The second source is an image source, necessary to fulfill the boundary condition, and it is located outside the medium at a distance $d = z_0 + 2z_b$, with the extrapolation length $z_b = (2/3)\, z_0\, A$ and A a constant that depends on the relative refractive index (e.g. $A(n_{eff}) = 4.22$, for $n_{eff} = 1.5$) [5, 22, 23]. The resulting $R(\rho)$ has the form:

$$\begin{aligned} R(\rho) \propto \frac{1}{4\pi}\Big(z_0(\mu_{\text{eff}} + \frac{1}{r_1})\frac{\exp(-\mu_{\text{eff}} r_1)}{r_1^2} \\ +(z_0 + 2z_b)(\mu_{\text{eff}} + \frac{1}{r_2})\frac{\exp(-\mu_{\text{eff}} r_2)}{r_2^2}\Big) \end{aligned} \tag{4.4}$$

where $r_1 = \sqrt{\rho^2 + z_0^2}$, $r_2 = \sqrt{\rho^2 + (z_0 + 2\ z_b)^2}$, and $\mu_{\text{eff}} = [3\mu_a(\mu_a + \mu_s')]^{1/2}$ is introduced as an effective attenuation coefficient, describing the joint effect of scattering and absorption [19].

The coefficients μ_s' and μ_a are combined in the constants z_0 and μ_{eff} defined above. Their effect on $R(\rho)$ is different: μ_s' determines the curvature and slope of $R(\rho)$ for short distances from the excitation point, whereas μ_a mainly affects the long range behavior of the reflected intensity.

The function $R(\rho)$ is the Green's function for intensity transport and allows to calculate the average reflected intensity function $\langle I_R(x,y)\rangle$ for an arbitrary illumination profile. Considering an illumination in the shape of a half-Gaussian beam, one obtains:

$$\begin{aligned}\langle I_{R\pm}(x,y)\rangle &= R(\rho) \otimes I_{\text{in}}(x',y') \equiv \\ &\equiv \iint R(\rho)\ H(\pm x')\ \exp(-\rho^2/w_{\text{in}}^2)\ dx'\ dy'\end{aligned} \tag{4.5}$$

where $H(\pm x')$ is the Heaviside step-function and w_{in} is the waist of the illumination beam. Equation (4.5) describes the knife-edge method we use later in this work, where incident light is provided in the shape of a half-Gaussian profile; for this case the two cross sections $\langle I_{R\pm}(x,y)\rangle$ and $I_{\text{in}}(x',y')$ are shown in Fig. 4.2 (a).

With the results in Eq. (4.5) we can now calculate the expected value for the speckles intensity variations $I_A(x,y)$:

$$I_A(x,y) \propto \langle |E_+(x,y)|\rangle\langle |E_-(x,y)|\rangle = \sqrt{\langle I_{R+}(x,y)\rangle\langle I_{R+}(-x,y)\rangle} \tag{4.6}$$

where we use the symmetry in our problem such that $\langle I_{R-}(x,y)\rangle = \langle I_{R+}(-x,y)\rangle$. The expression in Eq. (4.6) models the quantity $I_A(x,y)$ defined in Eq. (4.3), emerging from the interference of two fields, using the diffusion model for light transport in complex media. This equation is valid under the reasonable assumptions that the two fields $E_\pm(x,y)$ are uncorrelated and that the longitudinal coherence of the incident light is much longer than the diffuse optical path.

4.3 Experimental setup and samples

Setup description

A schematic of our experimental setup is shown in Fig. 4.1. Light from a HeNe laser (wavelength $\lambda = 632.8$nm) is delivered to the setup with a

single-mode fiber (not shown in Fig.4.3) and collimated for a beam waist of w_0 =1.6 mm. The beam is polarized in the x direction by polarizer P_0 and then reflected at normal incidence on a liquid crystal phase-only spatial light modulator (SLM) (Holoeye Pluto-VIS). The polarizer P_1 placed afterwards removes any minor depolarization introduced by SLM. In quasi-contact with the SLM we mount a knife-edge which can be moved into the optical path to block half of the beam.

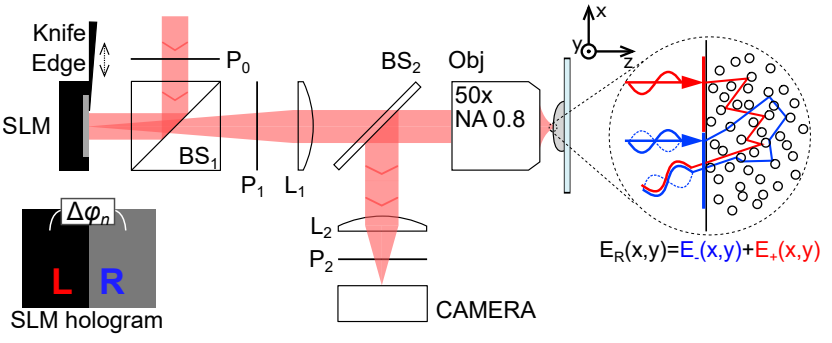

Figure 4.1: The experimental setup: a collimated laser (wavelength 633 nm) illuminates the spatial light modulator (SLM) after passing through the polarizer P_0. The wavefront-shaped light is polarized again with the polarizer P_1 and imaged on the sample with a telescope consisting of a tube lens L_1 (f=20 cm) and a 50x microscope objective.
The reflected light is collected with the same objective and its polarization is selected with the analyser P_2. A second tube lens L_2 (f = 20 cm) images the sample on a CCD camera. Bottom left: a scheme of the phase-step hologram projected on the SLM. Right: the interference between the light coming from the two halves of the SLM (red and blue lines) and exiting the sample at the same point.

The SLM surface is imaged onto the sample with a combination of a tube lens L_1 (focal length f = 20 cm) and a microscope objective (Nikon Epi Plan Fluor 50x, NA = 0.8) obtaining a final illumination spot with beam waist at the sample $w_{\text{in}} \simeq 31$ μm. This configuration allows to spatially define the phase over the incident wavefront. For convenience we choose the origin of the *(x,y)* coordinate system coincident with the center of the illumination spot. We image the sample in back-scattering geometry using the same objective and a second tube lens L_2 (f = 20 cm). We finally record an image of the sample with a CCD camera (Apogee Alta) after the analyser P_2 selects the measured linear polarization.

The sample is mounted on a 3-axis piezo stage for accurate positioning. A filtered halogen lamp provides the incoherent illumination used to focus

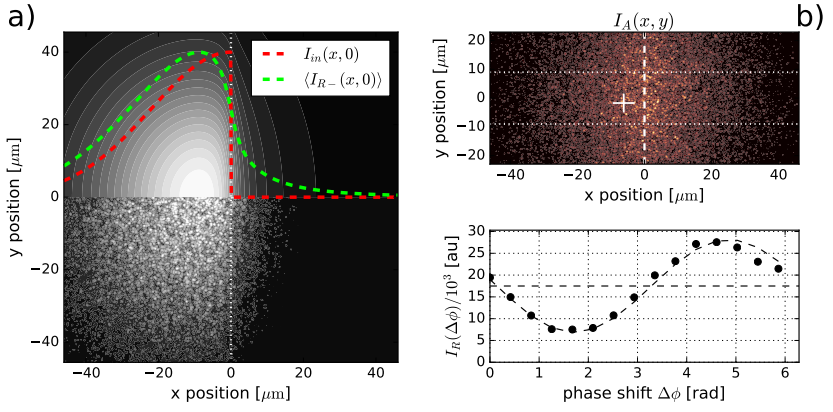

Figure 4.2: (a) Knife-edge method: the spatial speckles measured in reflection upon illumination with half a Gaussian beam (bottom part) are compared with the average speckle intensity pattern calculated with diffusion theory (top part). The two cross sections $I_{\rm in}(x,0)$ (red dashed line) and $\langle I_R(x,0)\rangle_\pm$ (green dashed line) from Eq. (4.5) are also shown. (b) Phase-step method: (Top) an example of measured speckle intensity variations $I_A(x,y)$ under phase-modulated illumination, with indicated the rectangular region used for ensemble averaging; (Bottom) the intensity as a function of the phase delay $\Delta\phi$ for the pixel pixel highlighted by a cross in the upper panel.

the sample; this avoids the appearance of speckles and allows to find regions where the sample appears flat and homogeneous within the field of view. We calculate the spatial resolution of the imaging system using the full width at half maximum of the spatial autocorrelation peak for the reflected speckle pattern, resulting in a value of $0.44\,\mu$m; this value is close to the expected diffraction limit of $0.40\,\mu$m and provides a resolution sufficient to resolve the spatial scale at which the reflected intensity decreases as an effect of diffusion.

Sample preparation

For our experiments we use three different scattering materials: dried liquid corrector (brand: Tipp-Ex) (sample 1), white paint (sample 2), and a disordered aggregate of polydisperse silica spheres (sample 3). Both samples 1 and 2 were stirred in form of suspension and deposited on a cleaned microscope slide and left to dry overnight at the room temperature. To prepare sample 3, we mixed thoroughly a suspension of silica micro-spheres (Sigma-Aldrich S5631) and deposited a few drops of the suspension on a cleaned objective substrate. The sample was then dried in an oven at 80 degrees for 30 minutes. The thickness of the samples are determined using with the microscope of our setup and have values, in the measurement regions, $h_1 = 640 \pm 6\ \mu$m, $h_2 = 290 \pm 4\ \mu$m,

$h_3 = 170 \pm 2$ μm, respectively. The overall thickness tolerance is estimated as 10%.

Experiment

We perform three different experiments (phase-step, knife edge and EBS) on each of the three samples and measure over multiple regions to verify consistency of the results. For the phase-step method, we project a phase-step hologram on the SLM with the step aligned at $x = 0$ on the sample. The projected hologram introduces a phase difference $\Delta\phi$ between the right and left side of the illumination spot. We image the reflected intensity $I_R(x, y, \Delta\phi_i)$ while applying $N = 15$ discrete phase-steps $\Delta\phi_i = i\frac{2\pi}{N}$ with $i = 0, \ldots, N-1$. By fitting Eq. (4.3) to the measured intensity as a function of $\Delta\phi_i$ for each pixel, we obtain the experimental values for the speckle intensity variations $I_A(x, y)$. The bottom plot in Fig. 4.2(b) shows $I_R(x, y, \Delta\phi_i)$ for a single pixel as a function of $\Delta\phi_i$.

The second approach is the knife-edge method, a diffuse imaging measurement. In this case half of the incident intensity profile is blocked with a knife-edge (see Fig. 4.1) obstructing the beam for $x > 0$, as described in Eq. (4.5). A typical intensity profile measured with sample 1 is shown in Fig. 4.2(a), where it is compared to the prediction obtained by numerically integrating Eq. (4.5). Note that the measurements show a speckle pattern, because we measure only for one specific realization of the random medium, whereas the diffusion theory only describes a smooth average intensity.

In the third method we measure the EBS cone of the samples using the setup described previously in Ref. [9]. The EBS cone appears on top of the diffuse reflection from the scattering media because of interference in the far field of counter-propagating optical paths in the medium. Experimental and theoretical work shows that the maximum intensity of the EBS cone is exactly two times the value of the diffuse reflected intensity and that the angular width of the cone depends on the transport mean free path of the scattering medium [8, 7].

To compare our measurements with both the models for phase-step and knife-edge methods we first average $I_A(x, y)$ and $I_-(x, y)$ along the y direction over a rectangular region, centred with the beam, spanning the full width of the images and limited to a band of $\Delta y = 18$ μm in the vertical direction (see Fig. 4.2(c)). In this region the diffuse reflected intensity modelled in Eq. (4.5) has almost no dependence on y. Since Δy is about $M = 40$ times wider

than the average speckles size, it is safe to assume that the average values $I_-(x) \equiv \langle I_-(x,y)\rangle_y$ and $I_A(x) \equiv \langle I_A(x,y)\rangle_y$ are equivalent to an ensemble average over different realizations of the scattering medium. The averaging also reduces the relative error on $I_-(x)$ and $I_A(x)$ by a factor $M^{-1/2}$.

The results we present for phase-step and knife-edge experiments are obtained detecting only the crossed-polarized backscattered light. This choice offers the advantage of removing the specular reflection of the sample surface, which conserves the incident linear polarization and is not accounted for by the diffusion model. Additionally, this also removes the stray light, originating from reflections from the optical components, in particular the microscope objective. We note that for all samples the reflected intensity in parallel and orthogonal polarization has about the same value, indicating that we are in the regime of nearly complete depolarization.

4.4 Results

The execution of the three experiments and subsequent data analysis are identical for all three samples: here we present the procedure applied to sample 2 (white paint) and only summarize the results for the other samples. The results for sample 2 are based on an average over $n = 4$ different positions. Ensemble averaging is further assured by the averaging along the y direction, as previously mentioned. For the EBS measurements we only present the final results.

To determine the transport and absorption mean free path it is necessary to know the effective refractive index n_{eff}. The values we use for n_{eff} for our three samples are approximate values and are listed in Table4.1. These value for n_{eff} are only parameter and are not critical when comparing three different methods. Real values can be measured with transmission measurements [24] or approximated with the effective medium theory [25].

In the phase-step experiment we measure $I_A(x,y)$, the speckle amplitude modulation defined in Eq. (4.6). In Fig. 4.3(a) we show the experimental curve $I_A(x) = \langle I_A(x,y)\rangle_y$ for sample 2, after averaging over four position on the sample surface and normalized to its values in proximity of $x = 0$. The measured $I_A(x)$ is symmetric around a maximum at $x = 0$, decaying almost exponentially with increasing distance form the phase step.

Using non-linear least-squares method, we fit the experimental data with the model in Eq. (4.6). The values of transport and absorption mean

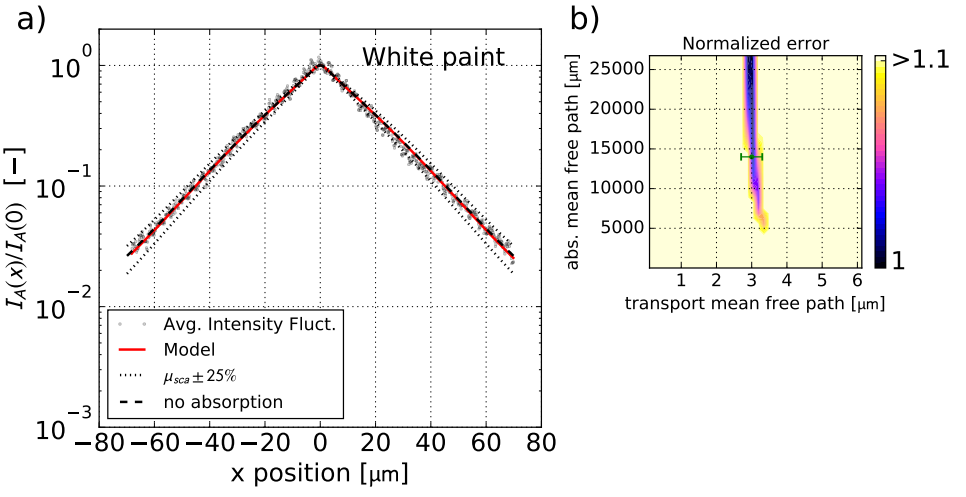

Figure 4.3: Phase-step results for the white paint. (a) Average speckle intensity modulation $I_A(x)$, normalized to its value at $x = 0$, for illumination with the phase-step positioned at $x = 0$. The red solid line shows the best fit curve with $l_{\mathrm{tr}} = 3.0$ μm and $l_a = 14$ μm. In the plot we also indicate the model with a transport coefficient altered by ±25% (dotted lines) and the model without absorption (dashed line). (b) The normalized error function in the parameter space (l_{tr}, l_a), calculated as defined in the text, with indication of the error minimum identifying the best fit parameters for the fit curve in panel (a), with the error bar for l_{tr}.

free path that fit the experimental data best are $l_{\mathrm{tr}} = 3.0 \pm 0.3$ μm and $l_a = 14.0 \pm 9$ mm, where the errorbars are given by the standard deviation calculated from the covariance matrix

The results of the knife-edge method are shown in Fig. 4.4(a), in the form of a typical average intensity profile $I_-(x) = \langle I_-(x, y)\rangle_y$ normalized to its value at $x = 0$. The measured curve shows a nearly half-Gaussian profile with a rounded top on the illuminated side and a diffuse intensity on the non-illuminated side, with its value decaying wit the distance from the knife edge.

We use Eq. (4.5) as model for the least square method; for sample 2 ($n_{\mathrm{eff}} = 1.4$) the best values for the transport and absorption mean free paths with this method are $l_{tr} = 2.6 \pm 0.1$ μm and $l_a = 19 \pm 6$ mm.

In Fig. 4.4(a) we also show, for comparison, the diffuse intensity profile of point-like illumination, instead of step-like, calculated with Eq. (4.4) using the best-fit parameters obtained from the knife-edge experiment. Fig. 4.4(a) clearly shows how the knife-edge illumination provides a more accurate view

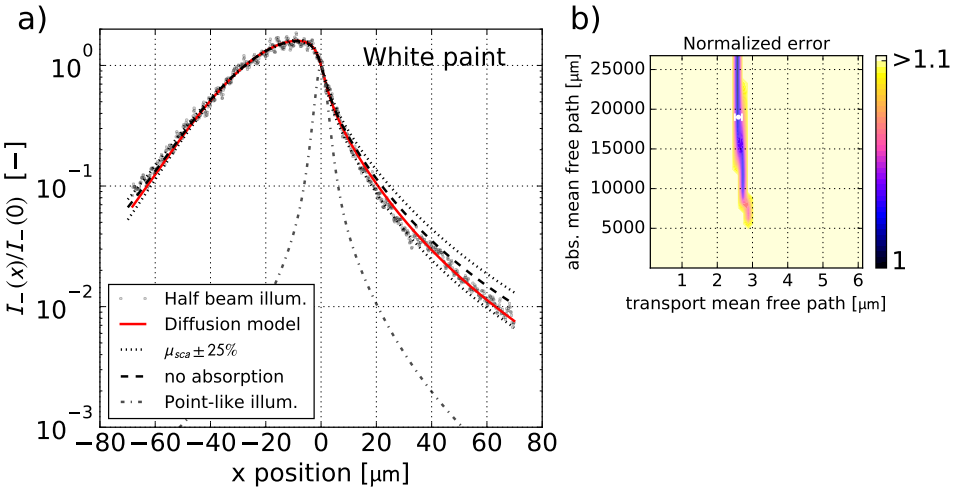

Figure 4.4: Knife-edge results for the white paint. (a) The average reflected intensity with half of the illumination spot blocked by the knife-edge. The intensity is averaged over the y direction over a $18\ \mu$m strip around the center of the illumination spot. Experimental data are fitted with the diffusion model in Eq. (4.5) to obtain the best fit parameters $l_{\rm tr}$ and l_a (in red). In the plot we also indicate the same model with a transport coefficient altered by $\pm 25\%$ (dotted lines), and the model without absorption (dashed line). The intensity profile for point-like illumination is plotted for comparison. (b) The normalized error function in the parameter space ($l_{\rm tr}$, l_a), calculated as defined in the text, with indication of the error minimum identifying the best fit parameters for the fit curve in panel (a), with the error bar for l_{tr}.

on the diffusion as a result of the dimensionality of the problem. For point illumination the intensity drops rapidly as it diffuses in two dimensions with average circular symmetry, whereas the knife-edge case has approximately a half-plane source and the intensity drops less steep as light diffuses only in one main direction.

The values of $l_{\rm tr}$ obtained from the two methods for Sample 2 are compatible within the error bars. In both cases, l_a is almost four orders of magnitude larger than $l_{\rm tr}$. In Table 4.1 we summarize the results for scattering and absorption parameters (for $\lambda = 632.8\,$nm) obtained from both methods on the three samples, and compare them to the EBS method. All samples show very low absorption and different scattering strengths, ranging from $l_{\rm tr} \simeq 0.75\ \mu$m for liquid corrector, to $l_{\rm tr} \simeq 5.0\ \mu$m for the aggregates of SiO_2 micro-spheres.

		Phase Step	Knife Edge	EBS
Sample 1 (Tipp-Ex)	$l_{\mathrm{tr}}[\mu\mathrm{m}]$	1.0 ± 0.4	0.75 ± 0.05	0.95±0.1
(n_{eff}=1.6)	l_a[mm]	5.3 ± 2.8	5.3 ± 1.1	
Sample 2 (white-paint)	$l_{\mathrm{tr}}[\mu\mathrm{m}]$	3.0 ± 0.3	2.6 ± 0.1	1.7±0.2
(n_{eff}=1.4)	l_a[mm]	14 ± 9	19 ± 6	
Sample 3 (SiO_2)	$l_{\mathrm{tr}}[\mu\mathrm{m}]$	5.0 ± 1.5	4.2 ± 0.5	2.9±0.3
(n_{eff}=1.4)	l_a[mm]	1±1	1 ± 0.4	

Table 4.1: Transport and absorption mean free paths l_{tr} and l_a for $\lambda = 632.8$ nm as determined from fits for three different measurement techniques: phase-step method, knife-edge method and enhanced back-scattering (EBS), with indicated n_{eff} assumed in the three methods for each sample.

4.5 Discussion

The phase-step method that we introduce to study the properties of a diffusive medium proves able to measure the transport mean free path for the three samples under study. We obtain values for l_{tr} that are similar to those calculated with the knife-edge experiment.

The results from the phase-step and knife-edge experiments agree within their error bars for all three samples. In the case of Tippex, the agreement extends also to the results of EBS, whereas for samples 1 and 2 the EBS yields lower values for l_{tr} than the other methods. The origin of this difference might be the different relative weights for long and short scattering paths in the (angular resolved) EBS measurements as compared to (spatially resolved) knife-edge and phase-step experiments.

The very low absorption in our samples, with l_a orders of magnitude higher than l_{tr}, makes it difficult to determine the absorption mean free path accurately, and it is only possible to give an upper limit for absorption. To visualize this, we report in Figs. 4.4(b) and 4.3(b) the error function between the model and the measurements in the parameter space (l_{tr},l_a), calculated as the sum of the squared residues for the logarithms of both model and experimental data $Err = \sum \left(ln(I_{fit}) - ln(I_{exp})\right))^2$ and normalized to its minimum value.

The two false-color plots show the normalized error function up to a value of $1 + 1/\sqrt{n \cdot M}$, with $n = 4$ number of averaged measured positions and M number of speckles over which averaging is performed. The error function plots indicate that, in our case, we can only determine a lower bound to l_a.

To help to understand how sensitive both methods are to l_{tr} and l_a, we also plot in Figs.4.4(a) and Fig.4.3(a) the models with virtually no absorption ($l_a = 10^6 \mu$m) and with l_{tr} modified by 25%.

One aspect that limits the accuracy of the calculation of transport and absorption mean free path with the phase-step method is, in our case, the size of the illumination spot. In our setup $w_0 \mu_{\text{eff}} \simeq 1 - 10$ and as a consequence illumination and diffused reflected light decay on the same spatial scale, making it more difficult to separate the two dynamics. By calculating the case of a half-plane illumination, obtained as the limit case of a Gaussian illumination with $w_0 \to \infty$, we noticed that the function $I_A(x)$ shows a more prominent dependence on the values of l_{tr} and l_a. This suggests that the use of high magnification objectives is not necessarily optimal for the phase-step method, as a larger illumination area might instead be preferred. We also note that a reduction of the collection NA increases the visibility of the spatial speckles, and thus the absolute value of $I_A(x)$ together with the signal to noise ratio, but at the price of a reduced resolution.

For both knife-edge and phase-step experiments we use results from the diffusion model, but the two techniques measure different quantities, the diffuse intensity and the speckle intensity modulation amplitude, respectively. This difference offers a potential advantages for the phase-step method over intensity modulation. First the dynamic range: the intensity observed in the knife-edge experiment depends on the square of the field $I_-(x) \propto |E_-(x)|^2$, and therefore decays faster away from $x = 0$ than the speckle intensity modulation $I_A(x)$, which depends linearly on the field $E_-(x, y)$. Weak fields are therefore easier to measure, similarly as in homodyne-detection schemes, as visible from the curves in Figs. 4.4 and 4.3. The second advantage of the phase-step method is that it is insensitive to a constant incoherent background, allowing for instance conventional microscopy images taken simultaneously. Finally, both our knife-edge and phase-step technique have an advantage over the more common diffuse imaging with spot-like illumination: by avoiding concentrating the input intensity in a focused spot they prevent the presence of non-linear optical effects and therefore also produce useful results while measuring the scattering properties of non-linear optical media.

We conclude our discussion with a technical remark on the use of the SLM. In many SLM-based experiments it is crucial to apply a position dependent phase correction to the SLM prior to the experiment in order to control the wavefront curvature. This is not necessary in our experiment, since the SLM is in the image plane of the sample and the measurements are based only on relative phase shifts rather than absolute phase value. Our experiment can even be performed without an SLM, using only a phase-step $\lambda/4$ plate on the image plane of the sample, centred with respect to the beam: rotating the plate by 180^0 around its axis produces an effective phase change of $\Delta\phi = \pi$ between the two halves of the beam. This is sufficient to measure the average amplitude variation of spatial speckles, although with a loss of signal-to-noise ratio of factor $\langle cos^2(\phi)\rangle^{-1} = 1/2$ with respect to our implementation. Finally, although we use a wavelength calibration for our SLM, this is also not strictly necessary as it can be calculated after the experiment from the intensity fluctuation of even a single pixel.

4.6 Conclusions

We have shown a new method to measure optical transport properties of a random scattering medium via illumination with phase-only modulated light. From the position dependence of the intensity modulation of the spatial speckle in reflection we are able to determine the transport mean free path and the absorption length. Better estimations would be possible in samples with shorter absorption mean free path but still in the diffusion regime, as for instance in biological tissues. All this is possible thanks to the linearity of the field transport and by implementing a numerical integration of the known diffusion model for light transport in random media.

The phase-modulation method has potential advantages over diffused imaging: it is not sensitive to incoherent background and offers the ability to investigate longer propagation lengths. Our method can be implemented in standard optical microscopes also without a SLM and is a viable non-invasive technique for studying materials and biological tissues.

Bibliography

[1] M. C. W. van Rossum and T. M. Nieuwenhuizen, *Multiple scattering of classical waves: microscopy, mesoscopy, and diffusion*, Rev. Mod. Phys. **71**, 313 (1999).

[2] R. H. J. Kop, P. de Vries, R. Sprik, and A. Lagendijk, *Observation of Anomalous Transport of Strongly Multiple Scattered Light in Thin Disordered Slabs*, Phys. Rev. Lett. **79**, 4369 (1997).

[3] J. G. Rivas *et al.*, *Optical transmission through strong scattering and highly polydisperse media*, EPL **48**, 22 (1999).

[4] P. M. Johnson *et al.*, *Time-resolved pulse propagation in a strongly scattering material*, Phys. Rev. E **68**, 016604 (2003).

[5] T. J. Farrell, M. S. Patterson, and B. Wilson, *A diffusion theory model of spatially resolved, steady-state diffuse reflectance for the noninvasive determination of tissue optical properties invivo*, Medical Physics **19**, 879 (1992).

[6] P. M. Johnson, T. van der Beek, and A. Lagendijk, *Diffuse imaging and radius dependent frequency correlations in strongly scattering media*, Optics Express **22**, 13330 (2014).

[7] P.-E. Wolf and G. Maret, *Weak Localization and Coherent Backscattering of Photons in Disordered Media*, Phys. Rev. Lett. **55**, 2696 (1985).

[8] M. P. V. Albada and A. Lagendijk, *Observation of Weak Localization of Light in a Random Medium*, Phys. Rev. Lett. **55**, 2692 (1985).

[9] O. L. Muskens and A. Lagendijk, *Broadband enhanced backscattering spectroscopy of strongly scattering media*, Optics Express **16**, 1222 (2008).

[10] J. W. Goodman, *Speckle phenomena in optics: theory and applications* (Roberts and Company Publishers) (2007).

[11] C. A. Thompson, K. J. Webb, and A. M. Weiner, *Diffusive media characterization with laser speckle*, Applied Optics **36**, 3726 (1997).

[12] J. D. McKinney, M. A. Webster, K. J. Webb, and A. M. Weiner, *Characterization and imaging in optically scattering media by use of laser speckle and a variable-coherence source*, Optics Letters **25**, 4 (2000).

[13] N. Curry *et al.*, *Direct determination of diffusion properties of random media from speckle contrast*, Optics Letters **36**, 3332 (2011).

[14] S. M. Popoff *et al.*, *Measuring the Transmission Matrix in Optics: An Approach to the Study and Control of Light Propagation in Disordered Media*, Phys. Rev. Lett. **104**, 100601 (2010).

[15] D. Akbulut *et al.*, *Optical transmission matrix as a probe of the photonic strength*, Phys. Rev. A **94**, 043817 (2016).

[16] I. M. Vellekoop, E. G. van Putten, A. Lagendijk, and A. P. Mosk, *Demixing light paths inside disordered metamaterials*, Optics Express **16**, 67 (2008).

[17] O. S. Ojambati *et al.*, *Coupling of energy into the fundamental diffusion mode of a complex nanophotonic medium*, New J. Phys. **18**, 043032 (2016).

[18] J. Bertolotti *et al.*, *Non-invasive imaging through opaque scattering layers*, Nature **491**, 232 (2012).

[19] A. Kienle *et al.*, *Spatially resolved absolute diffuse reflectance measurements for noninvasive determination of the optical scattering and absorption coefficients of biological tissue*, Applied Optics **35**, 2304 (1996).

[20] J. C. Dainty, in *Progress in Optics*, Vol. 14, edited by E. Wolf (Elsevier) (1977)

[21] A. Lagendijk, R. Vreeker, and P. De Vries, *Influence of internal reflection on diffusive transport in strongly scattering media*, Physics Letters A **136**, 81 (1989).

[22] R. C. Haskell *et al.*, *Boundary conditions for the diffusion equation in radiative transfer*, Journal of the Optical Society of America A **11**, 2727 (1994).

[23] R. Aronson, *Boundary conditions for diffusion of light*, Journal of the Optical Society of America A **12**, 2532 (1995).

[24] J. Gómez Rivas *et al.*, *Experimental determination of the effective refractive index in strongly scattering media*, Optics Communications **220**, 17 (2003).

[25] P. Chýlek *et al.*, *Light Scattering by Nonspherical Particles : Theory, Measurements, and Applications* (Academic Press) (2000).